CHAOS
Theory and Applications
in Applied Sciences and Engineering

e-ISSN: 2687-4539
RESEARCH ARTICLE
Vol.5 / No.2 / 2023 / pp.65-77
https://doi.org/10.51537/chaos.1262839

# Monitoring Blood Pressure Variability via Chaotic Global Metrics using Local Field Potential Oscillations

**David M. Garner**[α,β,1], **Shouyan Wang**[§,2], **Ashley L.B. Raghu**[§,3], **Vitor E. Valenti**[β,4], **Tipu Z. Aziz**[§,5] and **Alexander L. Green**[§,6]

[α]Cardiorespiratory Research Group, Department of Biological and Medical Sciences, Faculty of Health and Life Sciences, Oxford Brookes University, Headington Campus, Gipsy Lane, Oxford OX3 0BP, United Kingdom, [β]Autonomic Nervous System Center, Sao Paulo State University, UNESP, Marilia, SP, Brazil, [§]Nuffield Department of Surgical Sciences, Level 6, West Wing, John Radcliffe Hospital, Oxford University, Oxford OX3 9DU, United Kingdom.

## ABSTRACT

The intention was to associate blood pressure (BP) variability (BPV) measurements to Local field potentials (LFPs). Thus, assessing how LFPs can co-vary with BPV to permit implantable brain devices (via LFPs) to control output. Elevated BPV is a considerable cardiovascular disease risk factor. Often patients are resistant to pharmacotherapies. An alternative treatment is Deep Brain Stimulation (DBS). Mathematical techniques based on nonlinear dynamics assessed their correlation of BPV chaotic global metrics to LFPs. Chaos Forward Parameter (CFP6) was computed for LFPs, at three electrode depths in the mid-brain and sensory thalamus. Mean, root mean square of the successive differences (RMSSD) and the chaotic global metrics (CFP1 to CFP7) were computed for the BP signal. The right ventroposterolateral (RVPL) nucleus provided a substantial correlation via CFP6 for BP with R-squared up to approximately 79% by means of LFP gamma oscillations. Investigation of BPV via LFPs as a proxy marker might allow therapies to be attuned in a closed-loop system. Whilst all patients were chronic pain patients the chaotic global relationship should be unperturbed. LFPs correlation does not unconditionally predict its causation. There is no certainty DBS in these locations would be therapeutic but can be used as an assessment tool.

## KEYWORDS

Chaotic global metrics
*Spectral* multi-taper method
Blood pressure variabilty
Local field potentials
Deep brain stimulation

## INTRODUCTION

Monitoring deep brain local field potentials (LFPs) can provide wide-ranging information. They show oscillatory behaviour in several frequency bands. The frequency ranges explored here are delta (0.5-4 Hz), theta (4-8 Hz), alpha (8-12 Hz), beta (12-30 Hz), gamma (30-100 Hz) and fast (100-200 Hz) (McAfee 2017). They seed the electroencephalograms (EEGs) that are recorded non-invasively; so are clinically relevant. LFPs reflect the totalled synaptic activity from a local neuronal population within a region of about 100 micrometres located around the recording electrode. Implanted Deep Brain Stimulation (DBS) electrodes can be used to record their activity from precise areas of the brain. They have been targeted to within sub-millimetric accuracy. Such oscillations are relevant to the neurophysiological and neuropathological aspects of neuropathic pain (Ploner *et al.* 2017), dystonia (Whitmer *et al.* 2013) and Parkinson's disease (Dauer and Przedborski 2003; Lang and Lozano 1998; Stoco-Oliveira *et al.* 2021), amongst others. LFP oscillations in the different frequency ranges are created by distinct mechanisms but, are all related to neural synchrony.

Concentrating on blood pressure (BP) variability (BPV); elevated levels of BP and BPV are interesting because of their correlation with adverse cardiovascular and cerebrovascular events (Appiah *et al.* 2021). The cause of BPV fluctuations versus the LFPs from deep brain areas could provide a therapeutic solution using DBS, pharmacotherapies and so forth. These associations are upheld throughout all age and ethnic groups (Mancia *et al.* 2013). Despite numerous pharmacotherapies, fewer than 50% of

**Manuscript received:** 15 March 2023,
**Revised:** 4 May 2023,
**Accepted:** 5 May 2023.

[1]dgarner@brookes.ac.uk (**Corresponding author**)
[2]shouyan@fudan.edu.cn
[3]ashley.raghu@pmb.ox.ac.uk
[4]vitor.valenti@unesp.br
[5]tipu.aziz@nds.ox.ac.uk
[6]alex.green@nds.ox.ac.uk

hypertensive patients regulate their BP and variabilities effectively. Approximately 0.5% are refractory to treatment, implying uncontrollability despite taking up to five categories of anti-hypertensive medication (Calhoun *et al.* 2014).

Whilst mainstream clinical studies focus on intermittently measured, static BP measurements, BP is not a constant variable. It oscillates, exhibiting short-term (seconds to minutes), mid-term (hours to days) and long-term (between seasons) fluctuations (Parati *et al.* 2018; Webb *et al.* 2021). Likewise, it varies with circadian cycles (Frank *et al.* 1966). Clinical studies have established an independent relationship between both short and long term BPV (Parati *et al.* 2008) to cardiovascular events, regardless of their mean BP levels. These mentioned cardiovascular events and mean BP associations to the chaotic global techniques (discussed later) are expected to initiate from different areas of the midbrain. BPV deviations have been related to target organ damage, such as arterial stiffness (Kim *et al.* 2016; Zhou *et al.* 2018), left ventricular hypertrophy (Mustafa *et al.* 2016), risk of developing diabetic foot ulcers (Palatini 2018) and risk of pre- and post- surgical complications (Henriques *et al.* 2019; Jinadasa *et al.* 2018; Packiasabapathy *et al.* 2020; Rangasamy *et al.* 2020).

Treatment using antihypertensive medications may reduce BPV. Consequently, this is linked with optimal cardiovascular protection (Appiah *et al.* 2021; Corrao *et al.* 2011). This may have implications for stroke (Appiah *et al.* 2021; Rothwell *et al.* 2010), myocardial infarction, heart failure, peripheral artery disease, end-stage renal disease (Parati *et al.* 2012) and explicitly the dynamical diseases (Mackey and Milton 1987). Dynamical diseases are categorized by unexpected aberrations in the qualitative dynamics of physiological processes (Bernardo *et al.* 2014; Chang 2010). This causes irregular dynamics and pathological states. Accordingly, there is an association between the mathematical niche of nonlinear dynamics and complexity theory with clinical medicine (Belair *et al.* 1995).

Initially, we focussed on LFPs in six bandwidths: delta (0.5-4 Hz), theta (4-8 Hz), alpha (8-12 Hz), beta (12-30 Hz), gamma (30-100 Hz) and fast (100-200 Hz) in four anatomical locations and at three electrode depths. We computed the chaotic global metrics (Chaos Forward Parameter, CFP1 to CFP7) that assess the chaotic response and irregularities of datasets, as described by Garner and Ling in 2014 (Garner and Ling 2014). These methods were later advanced to investigate *high spectral* variants and applied them to mathematical inverse problems in 2021 (Garner and Ling 2021). They had already been applied to forward problems (Garner *et al.* 2020a, 2017). We computed the spectral multi-Taper Method (sMTM) for the LFPs. Then, we concurrently logged the mean, root mean square of the successive differences (RMSSD) (Nazaraghaei and Bhat 2020; Schmitt *et al.* 2015) and the non-trivial permutations of three chaotic global metrics of BP. We are assessing its BPV via the somewhat sinusoidally oscillating BP signal. This is analogous to the Duffing (Bonatto *et al.* 2008), Brusselator (Osipov and Ponizovskaya 2000) and Lorenz (Jeppesen *et al.* 2015) signals in Garner and Ling (Garner and Ling 2021).

BPV fluctuates highly irregularly and conceivably chaotically. So, algorithms that assess this property are appropriate. BPV arises as a result of the cross-talk between several cardiovascular and physiological regulatory systems. These include but are not limited to the baroreceptor reflex, the renin-angiotensin system, the vascular myogenic response and release of nitric oxide from the endothelium (Hocht 2013).

Up until now, the most sophisticated techniques applied to measure BPV have been their mean, standard deviation (Parati *et al.* 2013) and, Detrended Fluctuation Analysis (DFA) (Peng *et al.* 1995) in rats. Nonetheless, whilst DFA has been studied previously (Galhardo *et al.* 2009) it necessitates enforcement on the BP interpeak intervals not the periodic signal described here. Consequently, we later apply *high spectral* Detrended Fluctuation Analysis (*hs*DFA) as CFP5 instead. The chaotic global techniques implemented here (Barreto *et al.* 2014) are anticipated to have elevated responses to those changes than the linear time-domain descriptive statistics and DFA. Here, mean and RMSSD are set as benchmarks.

Some antihypertensive medications such as Calcium Channel Blockers (Rothwell *et al.* 2010; Silke *et al.* 1987) have been demonstrated to be effective in reducing BPV, either as monotherapy, or in combination with other therapies. Since diminishing BPV might avert the risk of cardiovascular mortality (Dolan and O'Brien 2010), under circumstances of refractory hypertension (Bacan *et al.* 2022; Matanes *et al.* 2022), an alternative treatment might be effective. Whilst not without significant risk, a potential substitute is DBS. DBS can effectively lower the absolute mean BP when stimulation is enforced to the ventral columns of the Periaqueductal grey area (PAG) (Green *et al.* 2005). BPV can fluctuate with chronic pain (Spallone 2018). So far, even if we can monitor the BPV levels via the LFPs; it is not inevitably the case that correlation implies causation. DBS in identical regions could be ineffective. Yet, additional pharmacotherapies should be analysed using these chaotic global techniques.

Anatomically, the periaqueductal grey matter (PAG) and rostrally contiguous periventricular grey (PVG) are located in the mid-brain and organized into functionally distinct and opposite columns (Carrive and Bandler 1991). These columns receive afferents from the sympathetic chain (Farkas *et al.* 1998), the rostral raphe (Marcinkiewicz *et al.* 1989), anterior hypothalamus (Cameron *et al.* 1995), thalamus (Krout and Loewy 2000) and cortex (Newman *et al.* 1989). In sequence, the PAG/PVG projects to sympathetic premotor neurons in the hypothalamus, pons and medulla. These projections influence sympathetic outflow that alter cardiovascular output (Farkas *et al.* 1998). Moreover, the PAG/PVG projects to vagal preganglionic neurons (Farkas *et al.* 1997). Assuming that the neurocircuitry of the PAG/PVG and their cross-talk components perform a pivotal role in cardiovascular control the central question of this study is whether the mathematical measures of complexity of this neural activity, in the appropriate region, correlate with BPV. Neuromodulation has the potential to reduce BPV and therefore reduce morbidity associated with this elevated BPV. The necessary neuromodulation may occur in very specific, sub-millimetric locations of the mid-brain and sensory thalamus.

## MATERIAL AND METHODS

Twenty-two human patients underwent DBS for neuropathic pain; all were chronic pain. All DBS implantations were performed at the John Radcliffe Hospital, Oxford, United Kingdom. The surgical procedures for the targeting and implantation of DBS electrodes (Model 3387, Medtronic, Minneapolis, MN, United States of America) have been described previously (Bittar *et al.* 2005). All subjects provided their informed written consent and confidentiality rights observed. This study was approved by the Oxford Local Ethics Committee (OxRecB): study number 05 Q1605 47 and conformed to the declaration of Helsinki.

### Data Acquisition & Experimental Procedures

The DBS electrodes were temporarily externalized for one week of trial stimulation. This delay was to ascertain if there was a clinical effect prior to implanting the battery. We recorded three bipolar recording signals in four different locations with each electrode situated either in the mid-brain or sensory thalamus (see Figure 1). Electrode contacts are labelled such that '0' is the deepest and '3' the most rostral so that bipolar channel (M23) was the most superficial, (M12) the middle depth and, (M01) the deepest of the recordings. The mid-brain regions were left and right periaqueductal/periventricular grey (LPVG & RPVG respectively). The thalamic areas were right and left ventroposterolateral nucleus (RVPL & LVPL respectively). In subjects with facial pain, their target was slightly medial and termed 'ventroposteromedial' nucleus or 'VPL' for simplicity as there is no structural or functional difference. This sensory thalamic location is ordered somatotopically with face medial and leg lateral (arm in between).

The researchers' ensured synchronisation between the BP signal and LFP measurements. The two outputs were logged simultaneously, aligned on the same clock and displayed online whilst recorded onto a hard disk in Spike2 (Cambridge Electronic Design, United Kingdom).

Datasets were acquired at two sampling frequencies; 4 kHz and 5 kHz. Those at 5 kHz were down-sampled to 4kHz so that all datasets could be manipulated identically. All signals were linearly detrended; the mean of the signal subtracted from the signal itself. The LFPs were bandpass filtered in accordance with delta (0.5-4 Hz), theta (4-8 Hz), alpha (8-12 Hz), beta (12-30 Hz), gamma (30-100 Hz) and fast (100-200 Hz). They were screened so that all values above and below four standard deviations were excluded from the time-series. This had the beneficial effect of removing the most extreme outliers without compromising the signal information. The blood pressure signal was Butterworth notch filtered to eliminate the 50 Hz UK mains noise. The width of the notch was defined by the 49 to 51 Hz frequency interval. This notch filter provided up to 24 dB of attenuation. The LFPs were not filtered in this way since they are only used to compute the sMTM (CFP6) which is contingent on the area between the power spectrum and the baseline, not the signal itself. (See later for elucidation on sMTM & CFP6). Next, all signals were down-sampled to 1 kHz so not too computer processor intensive when further processed. All time-series were 200 seconds long. To achieve correlations with LFP electrode recordings, we logged the concurrent blood pressure signals from the subjects. The LFPs and blood pressure signals had their power spectra computed for supplementary analysis. (See Figure 2).

An elevated level of chaotic global response is correlated with optimal physiological performance (Bernardo *et al.* 2014; De Souza *et al.* 2015). If the level of chaotic global response is lowered this is usually (there are exceptions) associated with the purported dynamical diseases (Belair *et al.* 1995; Mackey and Milton 1987; Pezard *et al.* 1996). These include cardiac arrhythmias and respiratory failures and are potentially fatal. Psychiatric disorders such as Schizophrenia (Bar *et al.* 2010, 2007) and bipolar disorder (Voss *et al.* 2006) are other examples. Chaotic global techniques have previously detected irregularities of the Heart Rate Variability (HRV) in attention deficit hyperactivity disorder (ADHD) (Wajnsztejn *et al.* 2016), type 1 diabetes mellitus (T1DM) (De Souza *et al.* 2015; Garner *et al.* 2017) and chronic obstructive pulmonary disease (COPD) (Bernardo *et al.* 2014). The restoration of HRV levels have been confirmed in subjects who have undergone Bariatric surgery (Benjamim *et al.* 2021). These novel chaotic global techniques to scrutinize BPV have not been applied to blood pressure signals prior to this study.

***Signal Processing of Data*** Regarding further analysis we enforced 100 seconds of time-series. This is since we evaluate half of the 200 second time-series by implementing a sliding window 20 times. Generally, by means of the standard techniques based on nonlinear dynamics such as Shannon Entropy (Shannon 2001) and DFA to assess HRV we require as a minimum of 5 to 20 minutes of time-series (Camm *et al.* 1996). Yet, with the use of chaotic global techniques an ultra-short time series has been proven to be adequate (Garner *et al.* 2019b). The *high spectral* chaotic global metrics are very sensitive and therefore further responsive to chaotic and irregular signals (Garner and Ling 2021).

Each recorded time-series was disconnected into 20 comparable epochs. This attained 20 values. This was to substantiate that if the measures of the linear regression increased. This would indicate that the two samples are more highly correlated. Each epoch incorporated half of the time-series with subsequent epochs being shifted forward by 2.5%. Therefore, the first epoch was measured from 0 to 50%, second from 2.5 to 52.5% and so on until the 20th epoch measured from 50 to 100%. We recorded three bipolar signals (M01 deepest, M12 middle, M23 most superficial) in four different locations of the mid-brain and sensory thalamus. This gave us 20 sections for each bipolar recording signal which were taken per data set.

With regards the LFPs, the sMTM (CFP6) of the 20 phases was taken for each section. This gave 20 values for (M01), 20 values for (M12) and 20 values for (M23) recordings for each of the four regions. The last channel of data to be processed was the blood pressure which was monitored concurrently with the bipolar electrode recordings. We separated this into 20 phases synchronously with the bipolar recordings. For the blood pressure, we computed the mean, RMSSD and the seven non trivial chaotic global metric combinations (CFP1 to CFP7). For a full chaotic global analysis all seven permutations are necessary. It is not sufficient to just equate the signal chaotic global values CFP5, CFP6 and CFP7. This corresponded to 20 for mean, 20 for RMSSD, 20 for CFP1 and so on up to and including 20 for CFP7.

The Multi-Taper Method (MTM) power spectrum provided the foundation for all calculations regarding CFP1 to CFP7 parameters. In this study the parameters for MTM are set at: (i) 1Hz for sampling frequency; (ii) time bandwidth for the DPSS is set to 4; (iii) FFT is the larger of 256 and the next power of two greater than the length of the segment (iv) Thomson's 'adaptive' nonlinear combination method to combine individual spectral estimates.

$$
\begin{aligned}
CFP1 &= \left[ n\left(hsEntropy\right)^2 + n\left(sMTM\right)^2 + \left(1 - \left[n\left(hsDFA\right)\right]\right)^2 \right]^{\frac{1}{2}} \\
CFP2 &= \left[ n\left(hsEntropy\right)^2 + \left(1 - \left[n\left(hsDFA\right)\right]\right)^2 \right]^{\frac{1}{2}} \\
CFP3 &= \left[ n\left(hsEntropy\right)^2 + n\left(sMTM\right)^2 \right]^{\frac{1}{2}} \\
CFP4 &= \left[ n\left(sMTM\right)^2 + \left(1 - \left[n\left(hsDFA\right)\right]\right)^2 \right]^{\frac{1}{2}} \\
CFP5 &= \left[ \left(1 - \left[n\left(hsDFA\right)\right]\right)^2 \right]^{\frac{1}{2}} \\
CFP6 &= \left[ n\left(sMTM\right)^2 \right]^{\frac{1}{2}} \\
CFP7 &= \left[ n\left(hsEntropy\right)^2 \right]^{\frac{1}{2}}
\end{aligned}
$$

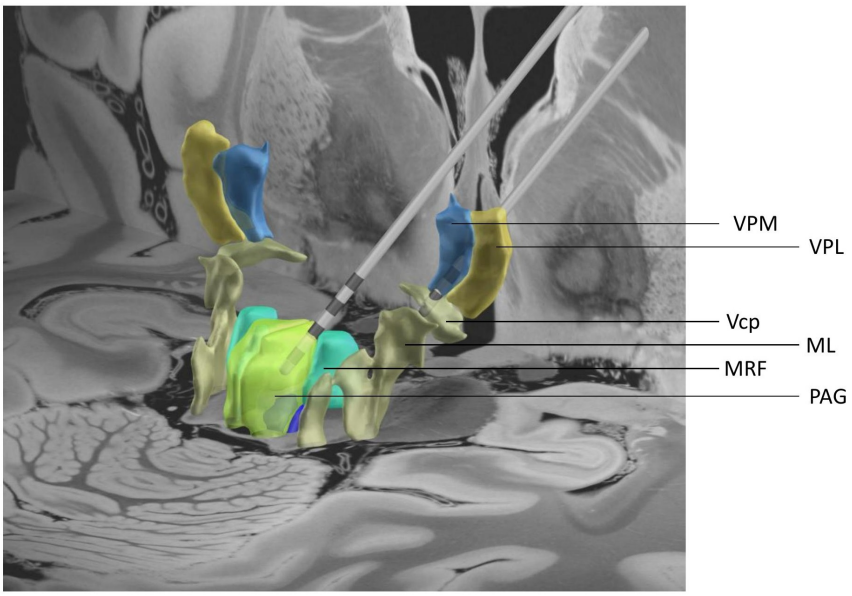


**Figure 1** A 3-Dimensional image of the electrode locations. One electrode is PAG/PVG and the other is in the sensory thalamus. These signify a 'mean' position for the cohort described. The coordinates are the mean target (middle 2 contact points) from the mid-commissural point in millimetres (mm). anterior commissure (AC) - posterior commissure (PC) coordinates. PAG array centre : X = 5mm, Y = -16mm, Z = -2mm. Thalamic electrode: X = 16mm, Y = -9mm, Z = 4mm. [PAG = periaqueductal grey, MRF = midbrain reticular formation, ML = medial lemniscus, Vcp = Ventro-caudalis parvocell, VPL = ventral posterolateral, VPM = ventral posteromedial].

***Multi-Taper Method Power Spectrum*** The MTM power spectrum is preferred and implemented as it has been established to statistically outperform several other power spectra (Alkan and Yilmaz 2007; Subasi 2007) when calculating chaotic global metrics (Garner *et al.* 2020a, 2017). MTM (Ghil 1997) is advantageous for spectral estimation and signal reconstruction, of a time-series of a spectrum that may contain broadband and line components. MTM is non-parametric as it does not enforce an a priori, parameter dependent model of the process that generated the time-series under analysis. It lessens the variances of spectral estimates by using a small set of tapers. Data is pre-multiplied by orthogonal tapers created to minimize the spectral leakage on account of the finite length of the time series. A set of independent approximations of the power spectrum is calculated. Functions identified as discrete prolate spheroidal sequences (DPSS) or Slepian sequences (Day *et al.* 2020; Slepian 1978) are a set of functions which optimize these tapers. They are defined as eigenvectors of a Rayleigh-Ritz minimization problem (Gould 1995). For further information consult Thomson (Thomson 1982) or Percival and Walden (Percival and Walden 1993).

***Statistical Assessments: Mean, RMSSD & Chaotic Global Variants*** Firstly, the sMTM (or CFP6) of the pre-processed (linearly detrended and bandpass filtered) LFPs signal was computed. This was for all three depths of electrode (M01, M12, M23), and at the four locations of the mid-brain (LPVG, LVPL, RPVG and RVPL). Secondly, we measured the mean and RMSSD of the blood pressure signal. These were the linear time-domain measurements. They are the simplest to compute, least computer processor intensive and are applied directly to the time-series. These two measurements could then be compared against the chaotic global metrics; key to this investigation. The linear metrics are applied as benchmarks to which all other chaotic global parameters are compared.

The motivation for implementing techniques founded on non-linear dynamics is that they measure the chaos and irregularity of responses in slightly different ways. The initial chaotic global metrics by Garner and Ling (2014) (Garner and Ling 2014) were later distinguished into their *high spectral* variants (Garner and Ling 2021), namely *high spectral* Entropy (*hs*Entropy) and *hs*DFA. These were demonstrated to be more responsive and influential on the basis of a multivariate statistical technique termed Principal Component Analysis (PCA) (Jolliffe 2005). They are functional with ultra-short time-series (Garner *et al.* 2019b). Here the time-series assessed are 100 seconds which is well within the range of the aforementioned study. Thus, the statistical hazards in the application of one are potentially compensated by the others in the CFP1 to CFP7 combinations. This is standard procedure when assessing chaotic global metrics (Bernardo *et al.* 2014; De Souza *et al.* 2015; Garner *et al.* 2022, 2020a, 2017).

*hs*Entropy is a function of the irregularity of amplitude and frequency of the power spectrums peaks. It is derived by applying Shannon entropy (Shannon 2001) to the MTM (Ghil 1997; Vautard *et al.* 1992) power spectrum. Such variability and introduction of errors from spectral leakage in the time-series and its mathematical relationships over the duration of the datasets are minimised by using the MTM power spectrum, as opposed to that of the Welch (Alkan and Kiymik 2006; Alkan and Yilmaz 2007) power spectrum, which has been applied previously (Bernardo *et al.* 2014; De Souza *et al.* 2015).

DFA (Peng *et al.* 1995) can be implemented to datasets where statistics such as mean, variance and autocorrelation fluctuate with time. To obtain the *hs*DFA the spectral adaptation is computed precisely as for *hs*Entropy. But, this time DFA is enforced onto the MTM power spectrum which has settings identified above. *hs*DFA responds to chaos and irregularities in the reverse way, so we subtract its value from unity; hence we enforce (1-*hs*DFA) when making comparisons.

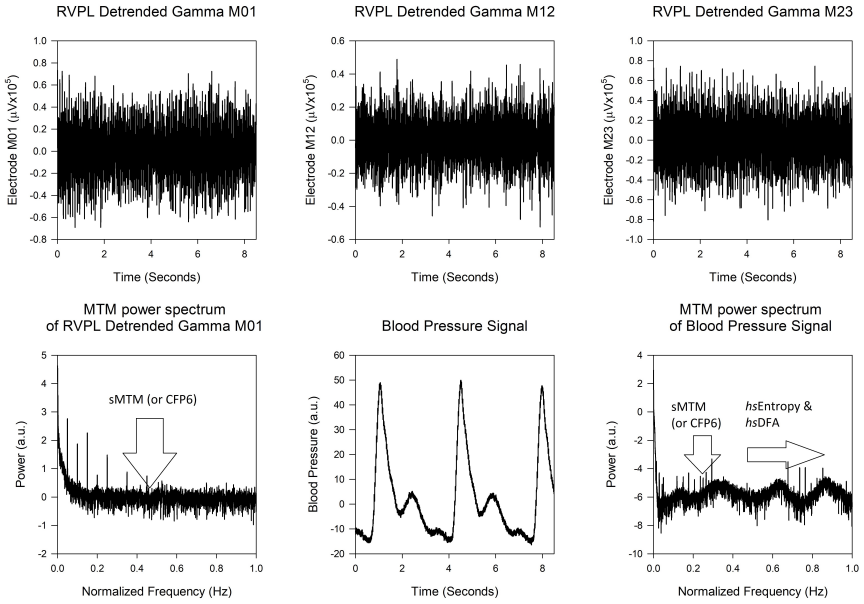


**Figure 2** Right ventroposterolateral (RVPL): Three bipolar electrode recording signals; linearly detrended by subtracting the mean of the signal from the signal itself. Then, bandpass filtered in the gamma region (30 to 100 Hz); Electrode M01 (a:upper left) Electrode M12 (b:upper middle) and Electrode M23 (c:upper right) all in units of microVolts. Next, Multi-Taper Method (MTM) Power Spectrum of RVPL linearly detrended Gamma M01 with sMTM (or CFP6) illustrated as the area under the vertical downwards pointing arrow of the power spectrum yet above the baseline (d:lower left) with power in arbitrary units; Blood Pressure signal (e:lower middle) in arbitrary units and time in seconds. MTM power spectrum of the Blood Pressure signal only with sMTM (or CFP6) again illustrated as the area under the vertical arrow of the power spectrum but above the baseline. *High spectral* Entropy (*hs*Entropy) and *high spectral* Detrended Fluctuation Analysis (*hs*DFA) labelled by enforcing Shannon Entropy and DFA onto the power spectrum, respectively as indicated by the horizontal arrow. Power in arbitrary units (f:lower right).

sMTM (CFP6) is the area between the MTM power spectrum and the baseline. MTM of a clean sinusoidal signal in continuous time and infinite length has zero area beneath it (Dirac 1939). For totally uniformly distributed random variables the spectrum is essentially flat. These lesser chaotic and irregular responses offer lower values and totally random data has a value of zero. Within these extremes, chaotic responses are often present with a continuous broadband spectrum. Broadband noise lifts peaks and the trend of the spectrum up and above the baseline, and so chaotic sets have greater values of sMTM. All three chaotic global metrics have identical weightings of unity throughout.

***Optimal bandwidth*** We assessed oscillatory performance using linear regressions during six frequency bands. These frequency ranges were delta (0.5-4 Hz), theta (4-8 Hz), alpha (8-12 Hz), beta (12-30 Hz), gamma (30-100 Hz) and fast (100-200 Hz). (See Figure 3). These regressions were also for the mean of the depth of electrodes (M01, M12, M23) for the four locations of the six aforesaid bandwidths. The gamma region achieved the highest level of linear regression. Therefore, indicating the strongest correlation. Accordingly, we enforce the 30 to 100 Hz bandwidth in all succeeding analysis.

***Goodness-of-Fit Assessments: Gamma region (30-100Hz)*** R-squared (Miles 2005) is referred to as the coefficient of multiple determination for multiple regression. It is a statistical method to assess the proportion of variance in the dependant variable that can be explained by an independent variable. Namely, how good does the data fit the regression model. R-squared is the variation divided by its total variation. R-squared is always between 0 and 1; or as a percentage, 0% and 100%. 0% percent indicates that the model explains none of the variability of the response data about its mean. Whilst, 100% specifies that the model explains all the variability of the response data about its mean.

Whilst R-squared delivers an insight into the assessment of the statistical model it ought not be relied upon alone. Further procedures need enforcement besides this technique. Moreover, it does not reveal information about the causal connection between the independent and dependent variables.

Residuals (Cook and Weisberg 1982; Gourieroux *et al.* 1987; Pierce and Schafer 1986) are useful for detecting outlying $y$ values. They verify the linear regression expectations in regard to the error term in the regression model. High-leverage values have smaller residuals as they often shift the regression line nearer to them. They can detect types of autocorrelations and heteroscedasticity.

Studentized residuals (Gray and Woodall 1994) provide an alternate measure for identifying outliers. They are more discriminative than the Raw, Pearson or Standardized residuals. The notion is to delete certain values in turn; each time refitting the regression model on the remaining ($n$-1) values. So, comparing the observed response values to their fitted values based on the models with the appropriate value deleted. Standardizing these deleted residuals attain the Studentized residuals. They are more effective at detecting outlying $y$ values than the other above-mentioned residuals.

We computed the mean of the standard deviation of the *modulus* of the Studentized Residuals and the mean of the maximum of the *modulus* of the Studentized Residuals. There were 20 residuals per regression. Residuals can be positive or negative and would cancel each other out if the mean was applied here just as they are. Consequently, we compute the modulus of the Studentized Residuals which indicates that all the negative values are made positive. Their individual magnitudes are unchanged. Then, since the outliers have greater values; be it the standard deviation or the

maximum; lower values indicate a better fit of regression.

Mean squared error (MSE) (Das *et al.* 2004; Tuchler *et al.* 2002; Wang and Bovik 2009) of an estimator calculates the mean of the squares of the errors. Intrinsically, the mean squared difference between the estimated values and the actual value. MSE is a function of risk, consistent with the expected value of the squared error loss. MSE is always above zero as there is always some randomness or noise inherent in the system. Again, lower values signify a better fit of regression.

## RESULTS

The objective is to obtain the highest R-squared. In Figure 3 we are considering the regressions between the LFPs sMTM (or CFP6) and one of the nine metrics; the mean, RMSSD and chaotic global metrics (CFP1 to CFP7) of BP. For each measure of the BP, we have four areas of mid-brain. When the location for the best regressions has been attained, we explore those with a positive $y$-intercept and a significant slope. These are for the LFPs in the gamma region (30-100Hz) and at three electrode depths (see Table 1). Negative $y$-intercepts indicate a negative chaotic response which is forbidden by the non-equilibrium laws of thermodynamics (Prigogine 1962). A significant slope is required for an adequate recorded response. A slope of zero would indicate a flat response, hence unresponsive and futile. With regards the standard deviation and maximum of the mean of modulus for the studentized residuals (see Figure 4a & Figure 4b); a lower value indicates a better fitted regression. MSE is also lowest for the optimal regression (see Figure 4c).

**LPVG: Left Periventricular Grey**

CFP2 (39-59%), CFP4 (31-55%), CFP6 (31-55%) and CFP7 (36-60%) are significant with R-squared between 31% and 60%. The slopes are fairly weak and unresponsive to the electrode depths. CFP2, CFP4, CFP6 and CFP7 all have positive y-intercepts.

CFP1 (19-35%), CFP3 (22-35%) and CFP5 (25-50%) have low values for R-squared. None of the CFPs cited are consistent with positive or negative slopes at all electrode depths.

CFP2, CFP4, CFP6 and CFP7 have very high standard deviation (0.5844-0.8060) and maximum (2.2352-3.1660) Studentized residuals and MSEs (0.0055-0.0083).

RMSSD at M23 has high standard deviation (0.6659-0.7264) and maximum (2.3182-2.6788). Studentized residuals and quite high MSEs (0.0072-0.0091). It is rejected on the basis of a flat response and these low goodness-of-fit values.

So, the regressions for LPVG are confirmed to be lower than most of the other locations.

**LVPL: Left Ventroposterolateral**

Mean (30-32%) and RMSSD (30-38%) values for R-squared are all low at 30% to 38%. CFP1 (16-32%), CFP2 (28-39%), CFP3 (17-32%) and CFP7 (30-39%) are rejected as they have low R-squared across all electrode depths.

CFP4 (32-47%) and CFP6 (33-47%) have quite low R-squared at 32% to 47%. Yet, CFP5 is rejected as it has negative y-intercepts throughout. Then, CFP4 and CFP6 slopes are fairly weak and so unresponsive to electrode depths. They give a flat response. None of the CFPs are consistent with positive or negative slopes at all electrode depths

CFP4 and CFP6 have very high standard deviation (0.6478-0.7790) and maximum (2.4447-2.9734) Studentized residuals and quite high MSEs (0.0016-0.0114).

Overall for LVPL, the regressions are low and the responses when the regression are high are flat and unresponsive.

**RPVG: Right Periventricular Grey**

Mean (not RMSSD) gives two robust values for R-squared at M01 (63%) and M12 (55%). CFP1 gives one strong value for R-squared of 54% at electrode location M01. But, the response is relatively flat too.

CFP2 (20-43%) and CFP7 (21-44%) are rejected as they give a low value for R-squared across all electrode depths. There are moderately significant values for R-squared CFP3 (39-58%), CFP4 (46-54%), CFP5 (55% only) and CFP6 (43-52%) are significant for R-squared at 39% to 58%. Yet, the slopes are steeper and are so are responsive with respect to all electrode depths. The Mean is consistent in that it has all y-intercepts positive for all electrode depths and very steep negative slopes. None of the CFPs or RMSSD are consistent as they respond with positive or negative slopes throughout at all electrode depths. Mean responds with all negative slopes.

All those with high R-squared CFP3, CFP4, CFP5 and CFP6 have moderately high standard deviation (0.6010-0.6377) and maximum (2.1023-2.4154) Studentized residuals and exceptionally low MSEs (<0.0001-0.0002).

**RVPL: Right Ventroposterolateral**

RMSSD (not mean) presents robust values for R-squared at M12 (66%) and M23 (56%). Nevertheless, they give low slopes so unresponsive with regards to the electrode depths. The response is flat and so rejected. CFP1 (16-36%) and CFP3 (19-41%) are rejected as they give a low value for R-squared across all electrode depths. CFP5 (39%) for M01 electrode only. All other electrodes gave a y-intercept which was negative and so forbidden.

CFP2 (44-57%), CFP4 (55-80%) and CFP6 (55-79%) gave strong R-squared and all positive y-intercepts throughout. Slopes are consistently negative for CFP2 and constantly positive for CFP4 and CFP6. CFP4 and CFP6 have the best R-squared at 55% to 80% and all slopes are similarly positive at all electrode depths.

CFP2 has high standard deviation (0.6062-0.6418) and maximum (2.2266-2.4339) Studentized residuals and relatively high MSE (0.0002-0.0021) compared to CFP4 and CFP6, later. CFP4 (SD 0.5307-0.6380; Max 2.0569-2.3452) and CFP6 (SD 0.5317-0.6364; Max 2.0349-2.3813) have low Studentized residuals and the low MSEs (0.0002-0.0008).

CFP7 (44-58%) for R-squared consistently negative slopes and always positive y-intercepts. CFP7 (SD 0.6009-0.6320; Max 2.2180-2.4339) have low Studentized residuals and the moderately low MSEs (0.0002-0.0021).

## DISCUSSION

The principal aim is to assess the relationship between BPV and LFPs using chaotic global metrics. A relationship between them has clinical implications in that (a) it may allow us to monitor LFPs via DBS electrodes and imply a specific BPV state that may be useful for monitoring or guiding therapy (b) it may imply (if causative) that DBS can be used to clinically alter BPV, and (c) whether DBS confirms suitable pharmacotherapies effective in absence of other designated techniques.

When assessing the regressions of CFP6 for the LFPs versus the mean, RMSSD and CFP1 to CFP7 for the BP signal, we established that the gamma region (30 to 100 Hz) had the highest R-squared which inferred the strongest correlation (See Figure 3).

LPVG and particularly LVPL have the weakest regressions throughout. This is the case for the mean, RMSSD and CFP1 to CFP7. Their slopes are weak and so their responses are flat. Their

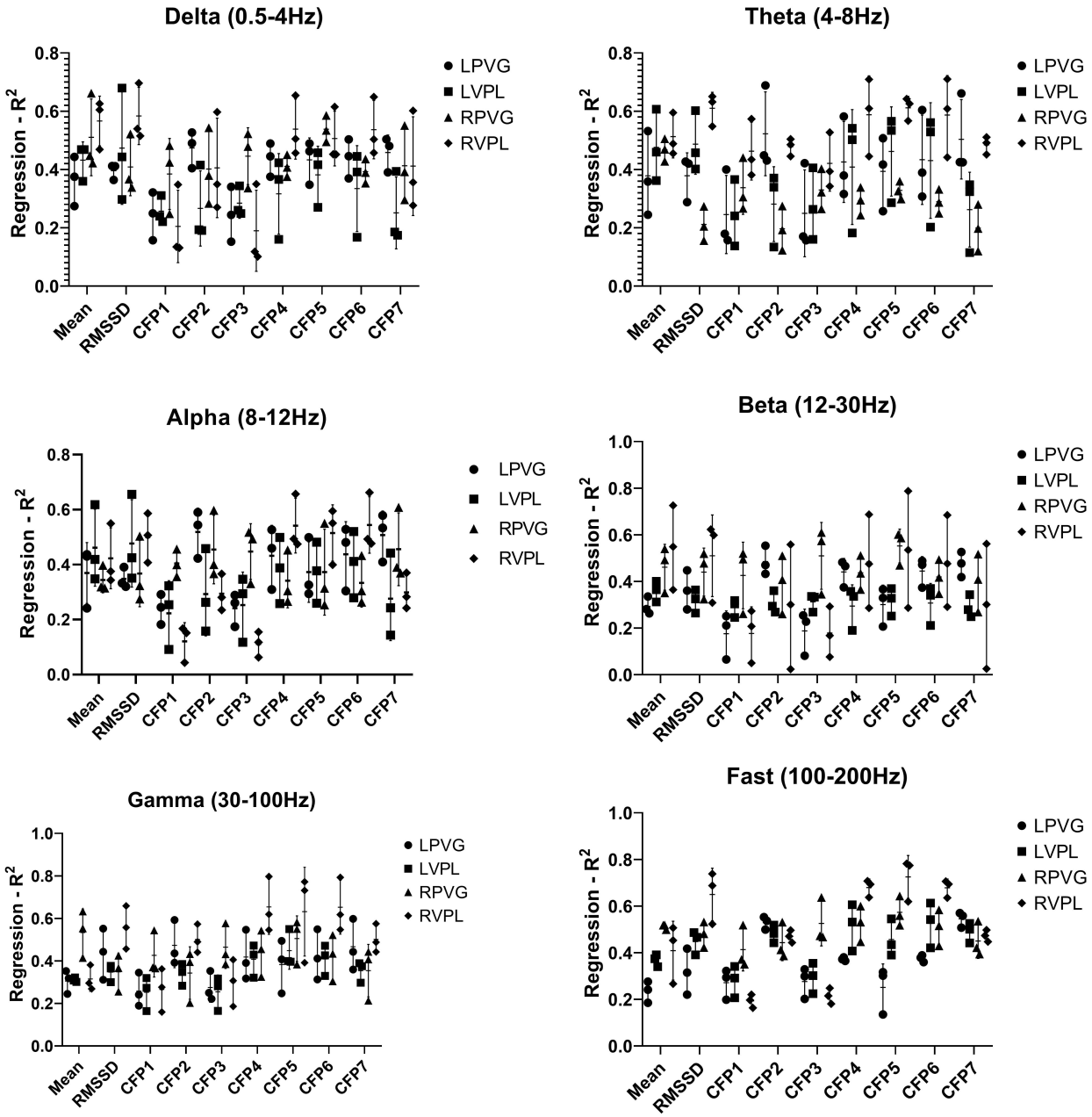


**Figure 3** Regressions (R-squared) of sMTM (CFP6) for Local Field Potentials (LFPs) in the delta (0.5-4 Hz), theta (4-8 Hz), alpha (8-12 Hz), beta (12-30 Hz), gamma (30-100 Hz) and fast (100-200 Hz) ranges for the mean of electrodes contacts [M01 (deepest depth), M12 (middle depth) and M23 (most superficial)] at four locations [LPVG (n=5), LVPL (n=5), RPVG (n=8) and RVPL (n=4)] versus the two linear descriptive (Mean & RMSSD) and the seven non-trivial permutations of the three *high spectral* chaotic global variant metrics (*high spectral* Entropy, *high spectral* Detrended Fluctuation Analysis (*hs*DFA) and spectral Multi-Taper Method (sMTM)) of the blood pressure signal (CFP1 to CFP7). The four symbols (circle, square, triangle and diamond) represent the level of R-squared for the LPVG, LVPL, RPVG and RVPL. There are three symbols describing the electrode contacts [M01, M12, M23]. The upper symbol is the maximum R-squared, the lower symbol the minimum R-squared and finally the middle symbol the median R-squared. The horizontal line between the maximum and minimum symbols represents their mean value.

**Table 1** Multi-Taper Method (MTM) Power Spectrum: Mean Regressions (R-squared), Mean Slopes and Mean Y-Intercepts of CFP6 for Local Field Potentials (LFPs) in the gamma range (30Hz to 100Hz) for the electrode contacts [M01 (deepest depth), M12 (middle depth) and M23 (most superficial)] versus the two linear descriptive (Mean and RMSSD) and the seven non-trivial permutations of the three *high spectral* chaotic global variant metrics (*high spectral* Entropy, *high spectral* Detrended Fluctuation Analysis and spectral Multi-Taper Method (sMTM)) of blood pressure (CFP1 to CFP7) for recordings from the mid-brain and sensory thalamus locations, namely LPVG (n=5), LVPL (n=5), RPVG (n=8) and RVPL (n=4).

| Gamma MTM | CFP (MTM) | Mean R-squared (Regression) | | | Mean Slope | | | Mean Y-Intercept | | |
|---|---|---|---|---|---|---|---|---|---|---|
| | | **M01** | **M12** | **M23** | **M01** | **M12** | **M23** | **M01** | **M12** | **M23** |
| LPVG (n=5) | **Mean** | 0.3189 | 0.3525 | 0.2449 | -0.0720 | -0.0155 | 0.0594 | 0.0686 | 0.0124 | -0.0583 |
| | **RMSSD** | 0.3116 | 0.4435 | 0.5523 | 0.0000 | -0.0003 | 0.0005 | 0.0065 | 0.0067 | 0.0061 |
| | **CFP1** | 0.2410 | 0.3450 | 0.1896 | -0.5489 | -0.0774 | 0.3674 | 1.4466 | 0.9777 | 0.5778 |
| | **CFP2** | 0.4359 | 0.5928 | 0.3919 | -1.0948 | 0.0418 | 0.4259 | 1.8926 | 0.7694 | 0.4505 |
| | **CFP3** | 0.2502 | 0.3531 | 0.2217 | -0.5537 | -0.0874 | 0.4114 | 1.4481 | 0.9837 | 0.5330 |
| | **CFP4** | 0.3177 | 0.5467 | 0.3906 | -0.1441 | -0.2564 | 0.2839 | 1.0639 | 1.1678 | 0.6629 |
| | **CFP5** | 0.2476 | 0.4947 | 0.4075 | -1.4032 | 4.1011 | 4.0996 | 1.9084 | -3.4154 | -3.6113 |
| | **CFP6** | 0.3132 | 0.5492 | 0.4113 | -0.1534 | -0.2787 | 0.3772 | 1.0659 | 1.1819 | 0.5677 |
| | **CFP7** | 0.4431 | 0.5979 | 0.3597 | -1.1093 | 0.0220 | 0.5019 | 1.9072 | 0.7877 | 0.3801 |
| LVPL (n=5) | **Mean** | 0.3222 | 0.3082 | 0.3015 | -0.0111 | 0.0368 | -0.0064 | 0.0055 | -0.0329 | 0.0086 |
| | **RMSSD** | 0.3768 | 0.3650 | 0.3001 | -0.0001 | -0.0009 | -0.0005 | 0.0064 | 0.0072 | 0.0067 |
| | **CFP1** | 0.2736 | 0.3194 | 0.1644 | 0.5669 | -0.5029 | -0.0449 | 0.3576 | 1.3904 | 0.9170 |
| | **CFP2** | 0.3481 | 0.3855 | 0.2834 | 1.1999 | -0.9483 | 0.0159 | -0.3325 | 1.7033 | 0.7151 |
| | **CFP3** | 0.2812 | 0.3173 | 0.1651 | 0.5730 | -0.5084 | -0.0493 | 0.3482 | 1.3935 | 0.9184 |
| | **CFP4** | 0.3215 | 0.4722 | 0.4298 | 0.0855 | -0.3483 | -0.1469 | 0.8465 | 1.2939 | 1.0808 |
| | **CFP5** | 0.3995 | 0.5500 | 0.3962 | 3.1834 | 7.6659 | 3.0033 | -2.3982 | -7.0839 | -2.4554 |
| | **CFP6** | 0.3296 | 0.4715 | 0.4263 | 0.0900 | -0.3570 | -0.1575 | 0.8347 | 1.2972 | 1.0850 |
| | **CFP7** | 0.3757 | 0.3891 | 0.2976 | 1.2406 | -0.9806 | 0.0075 | -0.3724 | 1.7352 | 0.7213 |
| RPVG (n=8) | **Mean** | 0.6332 | 0.5532 | 0.4144 | -17.3424 | -3.4684 | -35.1832 | 16.2967 | 2.5193 | 34.2220 |
| | **RMSSD** | 0.4248 | 0.2557 | 0.3664 | -0.1180 | 2.0073 | -1.7408 | 0.8548 | -1.2691 | 2.4785 |
| | **CFP1** | 0.5438 | 0.3699 | 0.3650 | 0.1079 | -2.5581 | 1.7963 | 0.8440 | 3.5045 | -0.8619 |
| | **CFP2** | 0.4326 | 0.2024 | 0.3948 | -0.2817 | -24.9221 | 15.1715 | 1.1101 | 25.7363 | -14.3729 |
| | **CFP3** | 0.5773 | 0.3853 | 0.4315 | 0.1508 | -4.1633 | 2.8160 | 0.7966 | 5.1043 | -1.8856 |
| | **CFP4** | 0.5428 | 0.3251 | 0.4554 | 0.0834 | 20.3526 | -14.4953 | 0.8200 | -19.4365 | 15.3966 |
| | **CFP5** | 0.5818 | 0.3833 | 0.5508 | 4.0876 | 68.1583 | -30.3918 | -3.3819 | -67.4462 | 31.1401 |
| | **CFP6** | 0.5216 | 0.3043 | 0.4340 | 0.1343 | 18.7723 | -13.5547 | 0.7770 | -17.8495 | 14.4640 |
| | **CFP7** | 0.4429 | 0.2134 | 0.4072 | -0.2136 | -28.9885 | 17.4886 | 1.0320 | 29.7911 | -16.6985 |
| RVPL (n=4) | **Mean** | 0.2692 | 0.3813 | 0.2958 | 11.3574 | -3.2315 | -1.4466 | -11.0458 | 3.0903 | 1.5040 |
| | **RMSSD** | 0.4570 | 0.6589 | 0.5576 | -0.1824 | 0.1025 | 0.0459 | 1.0476 | 0.7686 | 0.8224 |
| | **CFP1** | 0.3622 | 0.1597 | 0.2765 | -0.1647 | 0.0466 | 0.0496 | 1.1374 | 0.9384 | 0.9325 |
| | **CFP2** | 0.4902 | 0.4407 | 0.5731 | -0.7910 | -0.1683 | -0.3987 | 1.7010 | 1.1084 | 1.3244 |
| | **CFP3** | 0.4055 | 0.1861 | 0.3069 | -0.1954 | 0.0284 | 0.0188 | 1.1657 | 0.9546 | 0.9610 |
| | **CFP4** | 0.5458 | 0.6197 | 0.7973 | 0.4875 | 0.2878 | 0.5411 | 0.4723 | 0.6671 | 0.4227 |
| | **CFP5** | 0.3918 | 0.7319 | 0.7723 | -0.1385 | 2.1030 | 3.3639 | 0.5431 | -1.7147 | -2.9434 |
| | **CFP6** | 0.5474 | 0.6179 | 0.7930 | 0.4483 | 0.2641 | 0.5013 | 0.5140 | 0.6938 | 0.4651 |
| | **CFP7** | 0.4880 | 0.4426 | 0.5750 | -0.8580 | -0.2064 | -0.4636 | 1.7627 | 1.1422 | 1.3842 |

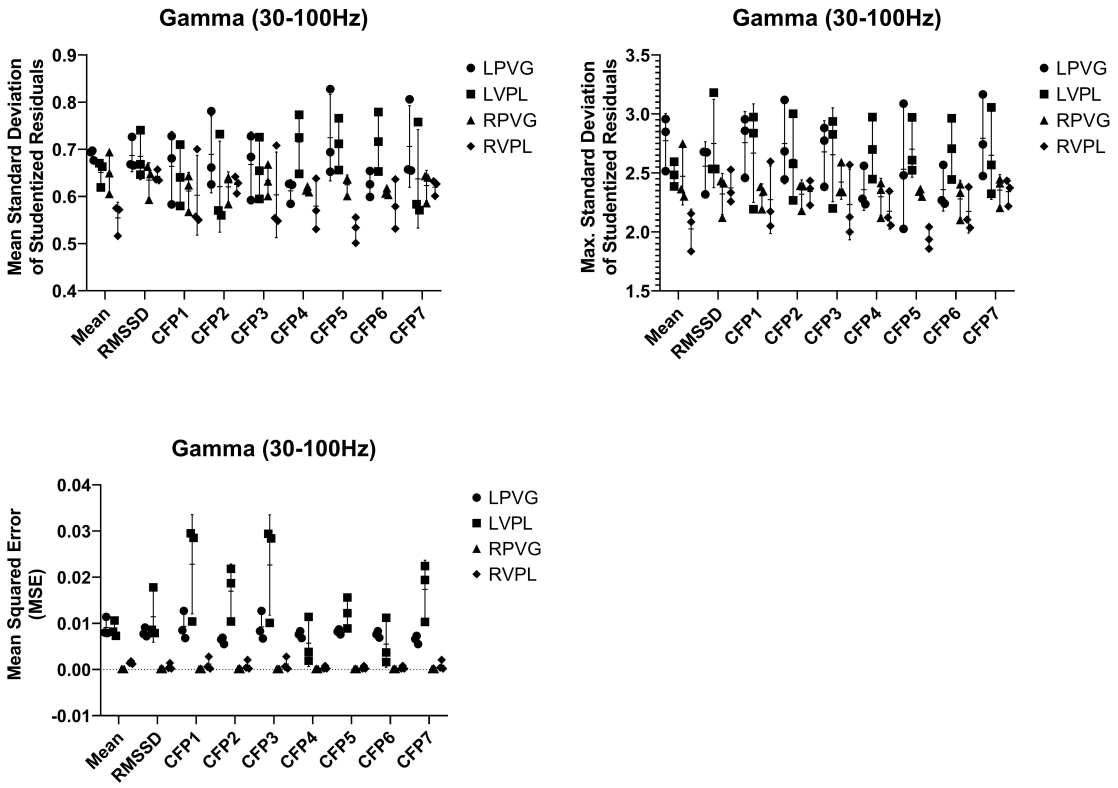


**Figure 4** (a: upper left) Mean of the Standard Deviation of the modulus of the Studentized Residuals (b: upper right) Mean of the Maximum of the modulus of the Studentized Residuals (c:lower left) Mean of the mean squared error (MSE); of spectral Multi-Taper Method (or CFP6) for LFPs in the gamma range (30 to 100Hz) for the electrode contacts at three depths [M01 (deepest), M12 (middle) and M23 (superficial)] versus the two linear descriptive (Mean & RMSSD) and the seven non-trivial permutations of the three *high spectral* chaotic global variant metrics (*hs*Entropy, *hs*DFA and sMTM) of blood pressure (CFP1 to CFP7) for recordings in the four areas, specifically LPVG (n=5), LVPL (n=5), RPVG (n=8) and RVPL (n=4). Again as with Figure 3. The four symbols (circle, square, triangle and diamond) represent appropriate values for the LPVG, LVPL, RPVG and RVPL. There are three symbols describing the electrode contacts [M01, M12, M23]. The upper symbol is the maximum, the lower symbol the minimum and finally the middle symbol the median. The horizontal line between the maximum and minimum symbols represents their mean value.

slopes are inconsistent throughout for both locations. Some slopes are negative, some positive. Their slopes are such that when the electrodes are surgically implanted for monitoring the different depths they give radically different results. Their goodness-of-fits via their Studentized residuals and MSE are poor. These highlight yet again that the regressions are less significant. The points form an excess of high residuals signifying that the model explains little of the variability of the response data around its mean. For LVPL, CFP5 is totally rejected as all y-intercepts are negative.

RVPL and RPVG are better sites for monitoring. They give higher values for their regressions throughout equated to LPVG and LVPL. With regards RPVG for CFP1 to CFP7 and RMSSD they are unreliable as they respond with positive or negative slopes at all electrode depths. Yet, their mean is dependable with all negative slopes. The slopes are steeper and are so are highly responsive regarding electrode depths. The mean is consistent in that it has all y-intercepts positive at all electrode depths. The mean, however, only measures the datas' magnitude and does not assess its sequence as with the nonlinear dynamic techniques. Therefore, it should be judged with caution.

For RVPL, RMSSD has high R-squared values at electrode locations M12 (66%) and M23 (56%) but at these locations they have low slopes; so unresponsive and flat. Slopes are moderately steep and consistently negative for CFP2. They are continually positive and quite steep for CFP4 and CFP6. As their slopes are consistent they are good locations to position electrodes since surgical precision is less critical. CFP2, CFP4 and CFP6 give positive values for their y-intercepts throughout. Their regressions are CFP4 (55-80%) and CFP6 (55-79%). These are the most significant regressions of all of the locations. But, RVPL could be unduly significant as a result of its low sample size.

We have demonstrated that the most statistically robust and significant combinations are CFP4 and CFP6 for RVPL with regressions significant at the level of about 55% to 80%. CFP1 and CFP3 are usually the most robust and statistically significant when applied to forward problems (Garner *et al.* 2019b, 2017; Wajnsztejn *et al.* 2016). Yet, CFP6 is favoured as it has been confirmed to be significant with forward and mathematical inverse problems, in particular, as in Garner and Ling (2014) (Garner and Ling 2014). Moreover, in 2021 with *high spectral* variants (Garner and Ling 2021). CFP6 is simple to implement and computationally fast.

Green *et al* in 2005 (Green *et al.* 2005) revealed that stimulation in the rostral PVG/PAG can increase or decrease levels of arterial blood pressure. This effect is contingent on the ventral/dorsal location of the electrode. In this study, we revealed that with recordings of RVPL, decreases in the blood pressure signal complexity can be monitored in a similar manner. It is important to realize the study by Green *et al* (Green *et al.* 2005) was considering BP whereas here we are assessing BPV. Interestingly the neuromodulation of BP and BPV are in different positions as revealed here. BPV neuromodulation is unique and so different LFPs are measured in dissimilar locations.

During some of the recorded LFPs time-series there were some locations in a few of the subjects which experienced short sections of DBS. These stimulations were not elongated enough to be measured for irregularities and chaotic responses. They are, nevertheless, not overlooked in the analysis. There were 20 epochs in the analysis which had a window of half of the entire time-series. This sliding window progresses from start to finish and for some zones or a few subjects this would have included short areas of DBS stimulation. These affect the LFPs recordings at three depths of electrode in the four areas of the brain. These were not excluded as their effects would be minimal. They cannot be spliced online which is the proposed format of the analysis. The LFPs would be principally resting but the zones of stimulation would improve the significance of the regressions by extending the statistical range of the LFPs. Each regression was computed from 20 points from the 20 sections. Next, a mean regression was computed for all the four locations. The number of subjects in the mean regression varied from four (RVPL) to eight (RPVG). The mean regression was used in the correlation of LFPs with BPV from the mean, RMSSD and chaotic global metrics.

It is important to understand that the human subjects in this study were all chronic pain patients. BP and BPV responses may be altered by chronic pain. Correspondingly, we should consider lateralisation (Hodgetts and Hausmann 2022; Hwang *et al.* 2022; Srinivasan *et al.* 2022). This is the inclination of some neural functions or cognitive processes to be located in one hemisphere of the brain instead of the other. There is lateralisation in BPV autonomic control.

If subjects experience Hypertension refractory to current pharmacotherapies, DBS may be a potential alternative treatment. DBS is a surgical procedure and as such cannot be performed without substantial risk and unanticipated difficulties. Whilst DBS of the PAG has been enforced to treat refractory Hypertension both in the context of pain (Patel *et al.* 2011) and without (O'Callaghan *et al.* 2017), its lack of use for this indication since our original conclusions in 2005 are possibly on account of this balance of risks. A potential correlation between the LFPs and BPV would be advantageous as it could be useful for developing adaptive forms of DBS (or novel pharmacotherapies) to reduce BPV using closed-loop feedback. The chaotic global sMTM (CFP6) could be a statistical marker.

Additionally, it would be wise to consider alternative neuromodulator therapies such as carotid body stimulation or renal sympathetic nerve ablation as they have lower risk. Both therapies failed phase three trials (Simplicity and BAROSTIM NEO Hypertension Pivotal Study ClinicalTrials.gov) for refractory Hypertension, but the latter is currently undergoing reassessment using specific patient cohorts and updated technology and techniques (SPYRAL HTN-ON MED Study ClinicalTrials.gov).

Further work could be commenced. For instance, the parameters for the MTM spectra could be adjusted. MTM was predominantly chosen as it has less spectral leakage. Yet, the manipulation of DPSS and Thomson's Multi-Taper settings have been repeatedly shown to be trivial (Garner *et al.* 2019a). Other methods of monitoring might be better. Levels of chaotic response could be assessed alternatively by the fractal dimensions of Higuchi (Garner *et al.* 2018; Nogueira *et al.* 2017) or Katz (Garner *et al.* 2018). Approximate (Garner *et al.* 2021b; Pincus 1995) and Sample (Richman and Moorman 2000) entropies could be computed. However, the latter two are excessively reliant on their embedding dimensions and tolerances. These cannot be attained in any systematic way which maintains them undependable (Garner *et al.* 2021b,a, 2020b). Also, they are usually enforced on the inter-beat intervals rather than just the oscillating signal as with chaotic global metrics.

## CONCLUSION

We revealed correlation (R-squared: up to 79%) in the RVPL site for all electrode depths (deep to superficial) between the LFPs gamma oscillations (30 to 100 Hz) and BPV for CFP6. This may have clinical uses. Perhaps, therapy could be achieved pharmacologically, surgically or otherwise by monitoring BPV using LFPs and making adjustments. Yet, correlation of the LFPs does not

inevitably predict its causation. There is no certainty that DBS in these areas will be therapeutic. They have only been confirmed for monitoring purposes with BPV. Further studies are suggested to ascertain if DBS or novel therapies do reduce BPV and lessen cardiovascular complications, potential morbidity and accordingly mortality.

#### Conflicts of interest

The authors declare that there is no conflict of interest regarding the publication of this paper.

#### Availability of data and material

Matlab code used in the study remains confidential as potential intellectual property.

#### Acknowledgements

This study was supported by the National Institute of Health (NIHR) Oxford Biomedical Research Centre.

## LITERATURE CITED

Alkan, A. and M. K. Kiymik, 2006 Comparison of `AR` and `Welch` methods in epileptic seizure detection. J Med Syst **30**: 413–9.

Alkan, A. and A. S. Yilmaz, 2007 Frequency domain analysis of power system transients using `Welch` and `Yule-Walker` `AR` methods. Energy conversion and management **48**: 2129–2135.

Appiah, K. O. B., M. Nath, L. Manning, W. J. Davison, S. Mazzucco, *et al.*, 2021 Increasing blood pressure variability predicts poor functional outcome following acute stroke. Journal of Stroke and Cerebrovascular Diseases **30**.

Bacan, G., A. Ribeiro-Silva, V. A. Oliveira, C. R. Cardoso, and G. F. Salles, 2022 Refractory hypertension: a narrative systematic review with emphasis on prognosis. Current Hypertension Reports **24**: 95–106.

Bar, K. J., S. Berger, M. Metzner, M. K. Boettger, S. Schulz, *et al.*, 2010 Autonomic dysfunction in unaffected first-degree relatives of patients suffering from schizophrenia. Schizophr Bull **36**: 1050–8.

Bar, K. J., M. K. Boettger, M. Koschke, S. Schulz, P. Chokka, *et al.*, 2007 Non-linear complexity measures of heart rate variability in acute schizophrenia. Clin Neurophysiol **118**: 2009–15.

Barreto, G. S., F. M. Vanderlei, L. C. M. Vanderlei, and D. M. Garner, 2014 Risk appraisal by novel chaotic globals to `HRV` in subjects with malnutrition. Journal of Human Growth and Development **24**: 243–248.

Belair, J., L. Glass, U. an der Heiden, and J. Milton, 1995 Dynamical disease: identification, temporal aspects and treatment strategies of human illness. Chaos: An Interdisciplinary Journal of Nonlinear Science **5**: 1–7.

Benjamim, C. J. R., Y. Mota de M. Pontes, F. Welington de Sousa Junior, A. A. Porto, C. R. Bueno Junior, *et al.*, 2021 Does bariatric surgery improve cardiac autonomic modulation assessed by heart rate variability: a systematic review. Surgery for Obesity and Related Diseases .

Bernardo, A. F., L. C. Vanderlei, and D. M. Garner, 2014 `HRV` analysis: A clinical and diagnostic tool in chronic obstructive pulmonary disease. Int Sch Res Notices **2014**: 673232.

Bittar, R. G., I. Kar-Purkayastha, S. L. Owen, R. E. Bear, A. Green, *et al.*, 2005 Deep brain stimulation for pain relief: a meta-analysis. J Clin Neurosci **12**: 515–9.

Bonatto, C., J. Gallas, and Y. Ueda, 2008 Chaotic phase similarities and recurrences in a damped-driven duffing oscillator. Phys.Rev.E.Stat.Nonlin.Soft.Matter Phys. **77**: 026217.

Calhoun, D. A., J. N. Booth III, S. Oparil, M. R. Irvin, D. Shimbo, *et al.*, 2014 Refractory hypertension: determination of prevalence, risk factors, and comorbidities in a large, population-based cohort. Hypertension **63**: 451–458.

Cameron, A. A., I. A. Khan, K. N. Westlund, K. D. Cliffer, and W. D. Willis, 1995 The efferent projections of the periaqueductal gray in the rat: A phaseolus vulgaris-leucoagglutinin study. `I. Ascending` projections. Journal of Comparative Neurology **351**: 568–584.

Camm, A., M. Malik, J. Bigger, G. Breithardt, S. Cerutti, *et al.*, 1996 Heart rate variability: standards of measurement, physiological interpretation and clinical use. task force of the european society of cardiology and the north american society of pacing and electrophysiology. Circulation **93**: 1043–1065.

Carrive, P. and R. Bandler, 1991 Viscerotopic organization of neurons subserving hypotensive reactions within the midbrain periaqueductal grey: a correlative functional and anatomical study. Brain research **541**: 206–215.

Chang, S., 2010 Physiological rhythms, dynamical diseases and acupuncture. Chin J Physiol **53**: 77–90.

Cook, R. D. and S. Weisberg, 1982 *Residuals and influence in regression*. New York: Chapman and Hall.

Corrao, G., A. Parodi, F. Nicotra, A. Zambon, L. Merlino, *et al.*, 2011 Better compliance to antihypertensive medications reduces cardiovascular risk. Journal of hypertension **29**: 610–618.

Das, K., J. Jiang, and J. Rao, 2004 Mean squared error of empirical predictor. The Annals of Statistics **32**: 818–840.

Dauer, W. and S. Przedborski, 2003 Parkinson's disease: mechanisms and models. Neuron **39**: 889–909.

Day, B. P., A. Evers, and D. E. Hack, 2020 Multipath suppression for continuous wave radar via slepian sequences. IEEE Transactions on Signal Processing **68**: 548–557.

De Souza, N. M., L. C. M. Vanderlei, and D. M. Garner, 2015 Risk evaluation of diabetes mellitus by relation of chaotic globals to `HRV`. Complexity **20**: 84–92.

Dirac, P., 1939 New notation for quantum mechanics. Proceedings of the Cambridge Philosophical Society **35**: 416.

Dolan, E. and E. O'Brien, 2010 Blood pressure variability clarity for clinical practice. Hypertension **56**: 179–181.

Farkas, E., A. S. Jansen, and A. D. Loewy, 1997 Periaqueductal gray matter projection to vagal preganglionic neurons and the nucleus tractus solitarius. Brain research **764**: 257–261.

Farkas, E., A. S. Jansen, and A. D. Loewy, 1998 Periaqueductal gray matter input to cardiac-related sympathetic premotor neurons. Brain research **792**: 179–192.

Frank, G., F. Halberg, R. Harner, J. Matthews, E. Johnson, *et al.*, 1966 Circadian periodicity, adrenal corticosteroids, and the eeg of normal man. J.Psychiatr.Res. **4**: 73–86.

Galhardo, C., T. Penna, M. A. de Menezes, and P. Soares, 2009 Detrended fluctuation analysis of a systolic blood pressure control loop. New Journal of Physics **11**: 103005.

Garner, D., M. Alves, B. da Silva, L. de Alcantara Sousa, and V. Valenti, 2020a Chaotic global analysis of heart rate variability following power spectral adjustments during exposure to traffic noise in healthy adult women. Russ J Cardiol **25**: 3739.

Garner, D., A. Bernardo, and L. Vanderlei, 2021a `HRV` analysis: Unpredictability of approximate entropy in chronic obstructive pulmonary disease. Series Cardiol Res **3(1)**: 1–10.

Garner, D., N. de Souza, and L. Vanderlei, 2020b Unreliability of approximate entropy to locate optimal complexity in diabetes mellitus via heart rate variability. Series Endo Diab Met. **2**: 32–40.

Garner, D., F. Vanderlei, L. Vanderlei, V. Valenti, C. J. R. Benjamim,

*et al.*, 2022 Chaotic global metric analysis of heart rate variability following six power spectral manipulations in malnourished children. Series Endo Diab Met. **4**: 44–58.

Garner, D. M., G. S. Barreto, V. E. Valenti, F. M. Vanderlei, A. A. Porto, *et al.*, 2021b HRV analysis: undependability of approximate entropy at locating optimum complexity in malnourished children. Cardiol Young pp. 1–6.

Garner, D. M., N. M. de Souza, V. E. Valenti, and L. C. M. Vanderlei, 2019a Complexity of cardiac autonomic modulation in diabetes mellitus: A new technique to perceive autonomic dysfunction. Romanian Journal of Diabetes Nutrition and Metabolic Diseases **26**: 279–291.

Garner, D. M., N. M. De Souza, and L. C. M. Vanderlei, 2017 Risk assessment of diabetes mellitus by chaotic globals to heart rate variability via six power spectra. Romanian Journal of Diabetes Nutrition and Metabolic Diseases **24**: 227–236.

Garner, D. M., N. M. de Souza, and L. C. M. Vanderlei, 2018 Heart rate variability analysis: Higuchi and katz's fractal dimensions in subjects with type 1 diabetes mellitus. Romanian Journal of Diabetes Nutrition and Metabolic Diseases **25**: 289–295.

Garner, D. M. and B. W. K. Ling, 2014 Measuring and locating zones of chaos and irregularity. J Syst Sci Complex **27**: 494–506.

Garner, D. M. and B. W.-K. Ling, 2021 Measuring and locating zones of chaos and irregularity by application of high spectral chaotic global variants. International Journal of Bifurcation and Chaos **31**: 2150236.

Garner, D. M., F. M. Vanderlei, V. E. Valenti, and L. C. M. Vanderlei, 2019b Non-linear regulation of cardiac autonomic modulation in obese youths: interpolation of ultra-short time series. Cardiol Young pp. 1–6.

Ghil, M., 1997 The SSA-MTM toolkit: Applications to analysis and prediction of time series. Applications of Soft Computing **3165**: 216–230.

Gould, S. H., 1995 *Variational methods for eigenvalue problems: an introduction to the methods of Rayleigh, Ritz, Weinstein, and Aronszajn*. Courier Dover Publications.

Gourieroux, C., A. Monfort, E. Renault, and A. Trognon, 1987 Generalised residuals. Journal of econometrics **34**: 5–32.

Gray, J. B. and W. H. Woodall, 1994 The maximum size of standardized and internally studentized residuals in regression analysis. The American Statistician **48**: 111–113.

Green, A. L., S. Wang, S. L. Owen, K. Xie, X. Liu, *et al.*, 2005 Deep brain stimulation can regulate arterial blood pressure in awake humans. Neuroreport **16**: 1741–5.

Henriques, T. S., M. D. Costa, P. Mathur, P. Mathur, R. B. Davis, *et al.*, 2019 Complexity of preoperative blood pressure dynamics: possible utility in cardiac surgical risk assessment. Journal of clinical monitoring and computing **33**: 31–38.

Hocht, C., 2013 Blood pressure variability: prognostic value and therapeutic implications. ISRN Hypertension **2013**.

Hodgetts, S. and M. Hausmann, 2022 in *Sex/Gender Differences in Brain Lateralisation and Connectivity*, Springer.

Hwang, W., D. Kang, and D. Kim, 2022 Brain lateralisation feature extraction and ant colony optimisation-bidirectional LSTM network model for emotion recognition. IET Signal Processing **16**: 45–61.

Jeppesen, J., S. Beniczky, P. Johansen, P. Sidenius, and A. Fuglsang-Frederiksen, 2015 Detection of epileptic seizures with a modified heart rate variability algorithm based on lorenz plot. Seizure **24**: 1–7.

Jinadasa, S. P., A. Mueller, V. Prasad, K. Subramaniam, T. Heldt, *et al.*, 2018 Blood pressure coefficient of variation and its association with cardiac surgical outcomes. Anesthesia & Analgesia **127**: 832–839.

Jolliffe, I., 2005 *Principal component analysis*. Wiley Online Library.

Kim, J.-S., S. Park, P. Yan, B. W. Jeffers, and C. Cerezo, 2016 Effect of inter-individual blood pressure variability on the progression of atherosclerosis in carotid and coronary arteries: a post hoc analysis of the normalise and prevent studies. European Heart Journal-Cardiovascular Pharmacotherapy **3**: 82–89.

Krout, K. E. and A. D. Loewy, 2000 Periaqueductal gray matter projections to midline and intralaminar thalamic nuclei of the rat. Journal of Comparative Neurology **424**: 111–141.

Lang, A. E. and A. M. Lozano, 1998 Parkinson's disease. New England Journal of Medicine **339**: 1130–1143.

Mackey, M. C. and J. G. Milton, 1987 Dynamical diseases. Ann N Y Acad Sci **504**: 16–32.

Mancia, G., R. Fagard, K. Narkiewicz, J. Redon, A. Zanchetti, *et al.*, 2013 2013 esh/esc guidelines for the management of arterial hypertension: the task force for the management of arterial hypertension of the european society of hypertension (esh) and of the european society of cardiology (esc). Blood pressure **22**: 193–278.

Marcinkiewicz, M., R. Morcos, and M. Chretien, 1989 CNS connections with the median raphe nucleus: Retrograde tracing with wga-apohrp-gold complex in the rat. Journal of Comparative Neurology **289**: 11–35.

Matanes, F., M. B. Khan, M. Siddiqui, T. Dudenbostel, D. Calhoun, *et al.*, 2022 An update on refractory hypertension. Current Hypertension Reports **24**: 225–234.

McAfee, S. S., 2017 *Assessing Neuronal Synchrony and Brain Function Through Local Field Potential and Spike Analysis*. Thesis.

Miles, J., 2005 R-squared, adjusted r-squared. Encyclopedia of statistics in behavioral science .

Mustafa, E. R., O. Istratoaie, and R. Musetescu, 2016 Blood pressure variability and left ventricular mass in hypertensive patients. Current health sciences journal **42**: 47.

Nazaraghaei, F. and K. K. Bhat, 2020 Physiological impacts of ajapa-japa yogic meditation on HRV index, RMSSD, PNN50, heart rate and GSR following three-month training course in comparison to FG meditation. Journal of Advanced Medical Sciences and Applied Technologies **5**.

Newman, D., S. Hilleary, and C. Ginsberg, 1989 Nuclear terminations of corticoreticular fiber systems in rats; pp. 253-264. Brain, behavior and evolution **34**: 253–264.

Nogueira, M. L., D. M. Garner, F. M. Vanderlei, L. C. de Abreu, and V. E. Valenti, 2017 Higuchi fractal dimension applied to rr intervals during exposure to musical auditory stimulation. Indian J Physiol Pharmacol **61**: 211–218.

O'Callaghan, E. L., E. C. Hart, H. Sims-Williams, S. Javed, A. E. Burchell, *et al.*, 2017 Chronic deep brain stimulation decreases blood pressure and sympathetic nerve activity in a drug-and device-resistant hypertensive patient. Hypertension **69**: 522–528.

Osipov, V. and E. Ponizovskaya, 2000 Stochastic resonance in the brusselator model. Phys.Rev.E.Stat.Phys.Plasmas.Fluids Relat Interdiscip.Topics. **61**: 4603–4605.

Packiasabapathy, S., V. Prasad, V. Rangasamy, D. Popok, X. Xu, *et al.*, 2020 Cardiac surgical outcome prediction by blood pressure variability indices poincare plot and coefficient of variation: a retrospective study. BMC anesthesiology **20**: 1–12.

Palatini, P., 2018 Risk of developing foot ulcers in diabetes: contribution of high visit-to-visit blood pressure variability. Journal of hypertension **36**: 2132–2134.

Parati, G., G. Bilo, and M. Valentini, 2008 Blood pressure vari-

ability: methodological aspects, pathophysiological and clinical implications. Manual of Hypertension of the European Society of Hypertension p. 61.

Parati, G., J. E. Ochoa, and G. Bilo, 2012 Blood pressure variability, cardiovascular risk, and risk for renal disease progression. Current hypertension reports **14**: 421–431.

Parati, G., J. E. Ochoa, C. Lombardi, and G. Bilo, 2013 Assessment and management of blood-pressure variability. Nature Reviews Cardiology **10**: 143–155.

Parati, G., G. S. Stergiou, E. Dolan, and G. Bilo, 2018 Blood pressure variability: clinical relevance and application. The Journal of Clinical Hypertension **20**: 1133–1137.

Patel, N., S. Javed, S. Khan, M. Papouchado, A. Malizia, *et al.*, 2011 Deep brain stimulation relieves refractory hypertension. Neurology **76**: 405–407.

Peng, C. K., S. Havlin, H. E. Stanley, and A. L. Goldberger, 1995 Quantification of scaling exponents and crossover phenomena in nonstationary heartbeat time series. Chaos **5**: 82–7.

Percival, D. and A. Walden, 1993 *Spectral Analysis for Physical Applications: Multitaper and Conventional Univariate Techniques*. Cambridge University Press, New York.

Pezard, L., J.-L. Nandrino, B. Renault, F. El Massioui, J.-F. Allilaire, *et al.*, 1996 Depression as a dynamical disease. Biological Psychiatry **39**: 991–999.

Pierce, D. A. and D. W. Schafer, 1986 Residuals in generalized linear models. Journal of the American Statistical Association **81**: 977–986.

Pincus, S., 1995 Approximate entropy (apen) as a complexity measure. Chaos: An Interdisciplinary Journal of Nonlinear Science **5**: 110–117.

Ploner, M., C. Sorg, and J. Gross, 2017 Brain rhythms of pain. Trends in cognitive sciences **21**: 100–110.

Prigogine, I., 1962 *Non-equilibrium statistical mechanics.*. New York: Interscience.

Rangasamy, V., T. S. Henriques, X. Xu, and B. Subramaniam, 2020 Preoperative blood pressure complexity indices as a marker for frailty in patients undergoing cardiac surgery. Journal of cardiothoracic and vascular anesthesia **34**: 616–621.

Richman, J. S. and J. R. Moorman, 2000 Physiological time-series analysis using approximate entropy and sample entropy. Am J Physiol Heart Circ Physiol **278**: H2039–49.

Rothwell, P. M., S. C. Howard, E. Dolan, E. O'Brien, J. E. Dobson, *et al.*, 2010 Effects of beta-blockers and calcium-channel blockers on within-individual variability in blood pressure and risk of stroke. The Lancet Neurology **9**: 469–480.

Schmitt, L., J. Regnard, and G. P. Millet, 2015 Monitoring fatigue status with HRV measures in elite athletes: an avenue beyond RMSSD. Frontiers in physiology **6**: 343.

Shannon, C. E., 2001 A mathematical theory of communication. ACM SIGMOBILE Mobile Computing and Communications Review **5**: 3–55.

Silke, B., M. A. Frais, K. A. Midtbo, S. P. Verma, S. Sharma, *et al.*, 1987 Comparative hemodynamic dose-response effects of five slow calcium channel-blocking agents in coronary artery disease. Clin Pharmacol Ther **42**: 381–7.

Slepian, S., 1978 Prolate spheroidal wave functions, fourier analysis and uncertainty, v, the discrete case. Bell Syst Tech J **57**: 1371–1430.

Spallone, V., 2018 Blood pressure variability and autonomic dysfunction. Current Diabetes Reports **18**: 137.

Srinivasan, V., N. Udayakumar, H. Liang, and K. Anandan, 2022 A hybrid approach for analysis of brain lateralisation in autistic children using graph theory techniques and deep belief networks. International Journal of Biomedical Engineering and Technology **39**: 40–64.

Stoco-Oliveira, M. C., A. L. Ricci-Vitor, L. M. Vanzella, H. B. Valente, V. E. d. S. Silva, *et al.*, 2021 Parkinson's disease effect on autonomic modulation: an analysis using geometric indices. Arquivos de Neuro-Psiquiatria **79**: 114–121.

Subasi, A., 2007 Selection of optimal AR spectral estimation method for eeg signals using cramer-rao bound. Comput.Biol.Med. **37**: 183–194.

Thomson, D. J., 1982 Spectrum estimation and harmonic analysis. Proceedings of the IEEE **70**: 1055–1096.

Tuchler, M., A. C. Singer, and R. Koetter, 2002 Minimum mean squared error equalization using a priori information. IEEE Transactions on Signal processing **50**: 673–683.

Vautard, R., P. Yiou, and M. Ghil, 1992 Singular-spectrum analysis - a toolkit for short, noisy chaotic signals. Physica D **58**: 95–126.

Voss, A., V. Baier, S. Schulz, and K. J. Bar, 2006 Linear and nonlinear methods for analyses of cardiovascular variability in bipolar disorders. Bipolar Disord **8**: 441–52.

Wajnsztejn, R., T. D. De Carvalho, D. M. Garner, L. C. M. Vanderlei, M. F. Godoy, *et al.*, 2016 Heart rate variability analysis by chaotic global techniques in children with attention deficit hyperactivity disorder. Complexity **21**: 412–419.

Wang, Z. and A. C. Bovik, 2009 Mean squared error: Love it or leave it: a new look at signal fidelity measures. IEEE signal processing magazine **26**: 98–117.

Webb, A. J., A. Lawson, K. Wartolowska, S. Mazzucco, and P. M. Rothwell, 2021 Progression of beat-to-beat blood pressure variability despite best medical management. Hypertension **77**: 193–201.

Whitmer, D., C. de Solages, B. C. Hill, H. Yu, and H. Bronte-Stewart, 2013 Resting beta hypersynchrony in secondary dystonia and its suppression during pallidal deep brain stimulation in DYT3+ l ubag dystonia. Neuromodulation: Technology at the Neural Interface **16**: 200–205.

Zhou, T. L., R. M. Henry, C. D. Stehouwer, T. T. van Sloten, K. D. Reesink, *et al.*, 2018 Blood pressure variability, arterial stiffness, and arterial remodeling: The maastricht study. Hypertension **72**: 1002–1010.

***How to cite this article:*** Garner, D. M., Wang, S., Raghu, A.L.B., Valenti, V.E., Aziz, T.Z., and Green, A.L. Monitoring Blood Pressure Variability via Chaotic Global Metrics using Local Field Potential Oscillations. *Chaos Theory and Applications*, 5(2), 65-77, 2023.